FFEMS Fatigue & Fracture of Engineering Materials & Structures
ORIGINAL CONTRIBUTION
doi: 10.1111/ffe.12401

# Numerical methods of multiaxial fatigue life prediction for elastomers under variable amplitude loadings

**J. CHUNG and N. H. KIM**

*Department of Mechanical and Aerospace Engineering, University of Florida, Gainesville, FL 32611, USA*

*Received Date: 12 May 2015; Accepted Date: 3 January 2016; Published Online: 23 February 2016*

**ABSTRACT** In this paper, numerical methods of fatigue life prediction for elastomers subjected to multidirectional, variable amplitude loadings are presented. Because experiments and numerical methods use different stress measures in large deformation, transformation between nominal stress and the second Piola–Kirchhoff stress is performed before fatigue life calculation. In order to incorporate the Mullins effect, the material properties of elastomers are calculated after an initial transition period. An efficient interpolation scheme using load stress/strain curves under unidirectional loading is proposed based on the fatigue characteristic of elastomers. A rainflow counting method with multi-stress components is developed for variable amplitude loadings, and the critical plane method is applied to find the plane with the maximum damage parameter. Fatigue life predictions using the proposed numerical method are validated against experimental results. As a practical example, the fatigue life of a rubber engine mount is predicted using the proposed numerical method.

**Keywords** critical plane method; elastomer; fatigue; Mullins effect; rainflow counting.

## NOMENCLATURE

| | |
|---|---|
| $d$ | = fatigue life prediction coefficients |
| $\mathbf{F}$ | = deformation gradient |
| $K$ | = fatigue life prediction coefficients |
| $m$ | = number of repeated loading blocks |
| $n$ | = number of peaks in a loading block |
| $\mathbf{n}_1, \mathbf{n}_2, \mathbf{n}_3$ | = eigenvectors of the right Cauchy Green deformation(C) |
| $\mathbf{n}_{L,1}, \mathbf{n}_{L,2}, \mathbf{n}_{L,3}$ | = eigenvectors of the logarithmic strain |
| $N_f$ | = number of cycles |
| $N_i$ | = number of life cycles |
| $\mathbf{P}$ | = first Piola Kirchhoff stresses(nominal stress) |
| $\mathbf{S}$ | = second Piola Kirchhoff stresses |
| $\mathbf{T}$ | = coordinate transformation matrix |
| $\alpha_i$ | = material constants for elastomer |
| $\mathbf{E}$ | = Green Lagrange strain |
| $\Delta\gamma_1$ | = range of shear strain on critical plane |
| $\Delta\tau_1$ | = range of shear stress on critical plane |
| $\Delta\varepsilon^{\max}$ | = range of maximum principal strain |
| $\Delta\varepsilon_1^{\max}$ | = range of nominal strain on critical plane |
| $\Delta\sigma_1$ | = range of nominal stress on critical plane |
| $\boldsymbol{\varepsilon}_{Eng}$ | = engineering strains |
| $\boldsymbol{\varepsilon}_{Log}$ | = logarithmic strains |
| $\lambda_i$ | = principal stretch |
| $\lambda_{L,1}, \lambda_{L,2}, \lambda_{L,3}$ | = eigenvalues of the logarithmic strain |
| $\mu_i$ | = shear modulus of elastomer |
| $\boldsymbol{\sigma}_G, \boldsymbol{\varepsilon}_G$ | = stress and strain of a free surface plane |

*Correspondence:* N. H. Kim, E-mail: nkim@ufl.edu


© 2016 Wiley Publishing Ltd.

$\boldsymbol{\sigma}_L$, $\boldsymbol{\varepsilon}_L$ = stress and strain of a candidate critical plane
$\Phi$ = eigenvector matrix of the right Cauchy Green deformation(C)
$\Phi_L$ = eigenvector matrix of the logarithmic strains

## INTRODUCTION

Elastomers, such as natural or synthetic rubber, are widely used in machine components for their energy-absorbing capability and elastic reversibility. Tyres, engine mounts for automobiles and rubber bearings for bridges are common examples of the elastomers' applications. These elastomers often have to endure cyclic loadings during their lifetime, and thus, fatigue failure is one of the critical issues in elastomer design. Although numerical methods of fatigue life calculation for metals are well developed, they are not directly applicable to elastomers due to the latter's nonlinear characteristics.[1]

Several experimental studies have suggested fatigue characteristics of elastomers, and a few numerical studies have performed in specific components of machinery. Wang *et al.*[2] studied multidirectional fatigue properties using a series of experiments for proportional and non-proportional loadings and compared their results with several fatigue criteria. Li *et al.*[3] and Kim *et al.*[4] studied the fatigue failure of a rubber component of automobiles using numerical and experimental methods, but the numerical methods were limited only on the test conditions. In terms of strain measures, Kim *et al.*[4] used the maximum principal Green–Lagrange strain, and Li *et al.*[3] used the maximum principal true strain for the damage parameter. Mars *et al.*[5–7] studied several damage parameters for fatigue of elastomers, which were related to strain and energy, and Saintier *et al.*[8,9] suggested an equivalent stress parameter, which included damage and reinforcement quantities on the critical plane. Zarrin-Ghalami *et al.*[10,11] studied experimental data and life prediction analysis for an automobile mount under constant and variable amplitude in in-phase and out-of-phase loading.

However, most studies are limited to constant amplitude proportional loadings and numerical methods used for comparing their fatigue parameters with test results. Studies of numerical methods for fatigue life prediction of practical elastomers subjected to multidirectional transient amplitude loading have rarely been reported, which is the main contribution of the paper.

Elastomers are known as a typical hyperelastic material having a nonlinear elastic behaviour, and thus, the superposition technique in a metal fatigue is not applicable for calculating dynamic stress/strain histories. This means that the computational cost of calculating stress/strain histories of elastomers under variable amplitude loading greatly increases because of the nonlinear transient analysis. Generally, material properties of fatigue life prediction are decided by experiments, which are based on nominal stress and strain. On the other hand, numerical methods of elastomers often use the second Piola–Kirchhoff stress and the Green–Lagrange strain, or Cauchy stress and logarithmic strain to describe the nonlinear behaviour of elastomers. In order to address this difference, a reliable conversion procedure between the two different measures is necessary for numerical methods of elastomers' fatigue. There are many damage parameters for fatigue life prediction: some of them have a single component, and others have multicomponents. In constant unidirectional loading, estimation of damage parameters is straightforward. However, in variable amplitude loading, the estimation of multicomponent damage parameters is a challenging task, and a modified rainflow counting technique is required. In this paper, practical numerical methods for fatigue life prediction of elastomers under time-varying loads are presented by addressing the aforementioned issues.

The paper is organized as follows. The first section describes properties of elastomers for fatigue prediction, such as mechanical characteristics, stresses and strains measures and damage parameters of fatigue prediction. The second section shows the numerical prediction of fatigue of elastomers using experimental condition and a practical example of an engine mount. Finally, conclusions are discussed in the last section.

## PROPERTIES OF ELASTOMERS FOR FATIGUE PREDICTION

### Characteristic properties of elastomers

Hyperelasticity is a characteristic property of elastomers, showing a nonlinear elastic behaviour as illustrated in Fig. 1. It does not have permanent plastic deformation, which means that elastomers can return to their original state when external loading is removed. Although elastomers show nonlinear behaviour, there is a one-to-one relation between the applied load and stress/strain.

In this paper, loadings used in fatigue prediction are classified into two categories to develop efficient methods for generating stress and strain histories. The first is unidirectional loading in which the dynamic load history can be parameterized by the history of a single load factor (e.g. see path 1 in Fig. 11). In such a case, a single nonlinear analysis

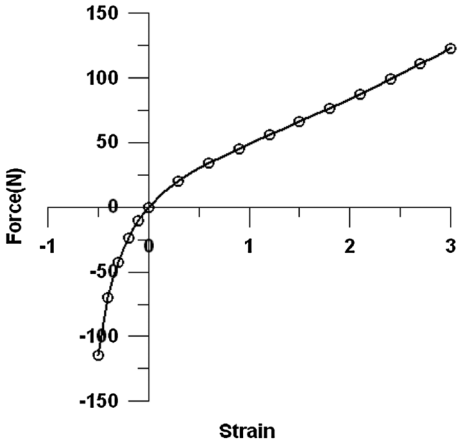


**Fig. 1** One-to-one relation between force and strain.

with increasing load factors from the minimum to the maximum can be used to interpolate the history of stress and strain, which can greatly reduce computational cost. The other is multidirectional loading, composed of several unidirectional loadings that do not have the same time-varying load factor. In multidirectional loading, the interpolation scheme cannot be used, and thus, nonlinear transient analysis that follows the complete load history is required to obtain stress and strain histories. If multidirectional loading has repeated loading blocks, then nonlinear transient analysis can be performed over a loading block to save computational efforts. Paths 2 and 3 in Fig. 11 are examples of multidirectional loading because they have axial and torsional loadings whose load factors vary independently.

The Mullins effect is an important characteristic property of elastomers.[7] This effect is caused by microscopic debonding of polymer particles chains. It is a particular damage behaviour in which the stress–strain curve relies on the maximum value of strain. The stress–strain path including the Mullins effect is shown in Fig. 2.

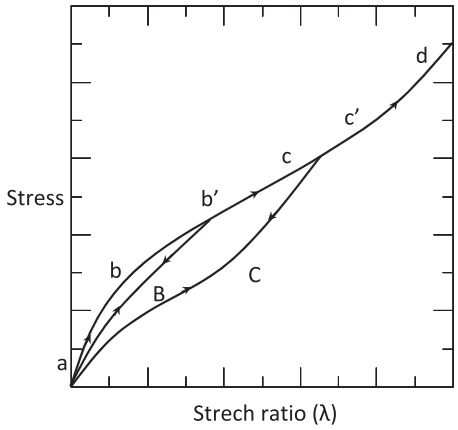


**Fig. 2** Stress–strain path including Mullins effect.

The stiffness against deformation is reduced according to the cyclic loadings; however, the reduction is stabilized within the first few loading cycles. Because a fatigue phenomenon occurs with thousands or millions of cycles, the material properties of the stabilized status after the Mullins effect should be used for fatigue calculation.

In this paper, the three-term Ogden model is used to express the strain energy density function as

$$W = \sum_{i=1}^{N} \frac{\mu_i}{\alpha_i}\left(\lambda_1^{\alpha_i} + \lambda_2^{\alpha_i} + \lambda_3^{\alpha_i} - 3\right) \tag{1}$$

where $\lambda_1, \lambda_2$ and $\lambda_3$ are principal stretches and $\mu_i$ and $\alpha_i$ are material properties of the elastomer. Table 1 lists the mechanical properties of an Ogden hyperelastic material as suggested by Wang *et al.*[2] The properties of elastomers considering the Mullins effect are estimated by comparing the stress values between the initial stage and the stabilized stage in the uniaxial fatigue tests performed by Wang *et al.*[2] Because stress linearly depends on $\mu_i$, in the Ogden model, a scale factor is applied to $\mu_i$ in order to consider the Mullins effect.

## Stresses and strains measures

In general, identifying material parameters through experiments should be independent of numerical methods; otherwise, it is possible to determine if the error in numerical methods may affect the identified material parameters. Even if elastomers experience large deformation, nominal stress and strain are always measured based on the forces and displacements during the test. On the other hand, hyperelastic models are often defined using different stress and strain measures, such as the second Piola–Kirchhoff stress and the Green–Lagrange strain. Therefore, there is a distinct discrepancy in stress and strain measures between experiments and numerical methods. In addition, fatigue damage parameters are also defined using nominal stress and strain because they were determined by experiments. As a result, it is necessary to convert the stress and strain measures of numerical methods to nominal stress and strain. The detailed conversion relations between numerical methods and experiments measures are listed in Appendix.

**Table 1** Material properties of the Ogden constitutive model

| | $\mu_1$ | $\alpha_1$ | $\mu_2$ | $\alpha_2$ | $\mu_3$ | $\alpha_3$ |
|---|---|---|---|---|---|---|
| Without Mullins effect | 0.5558 | 2.5786 | 5.6426 | 0.1068 | 6.2845 | 0.1120 |
| With Mullins effect | 0.4099 | 2.5786 | 4.1613 | 0.1068 | 4.6348 | 0.1120 |

### Damage parameters of fatigue life prediction

In general, the fatigue life of elastomers can be found by making a relationship between a damage parameter and the number of fatigue life cycles as in Eq. (2). Different damage parameters have been suggested: the SWT model by Smith *et al.*[12], the CXH model by Chen *et al.*[13] and the modified Fatami–Socie's model by Fatami and Socie.[14] Because the purpose of the paper is to develop a general computational framework for fatigue analysis of elastomer, different fatigue life prediction models can be used. In this study, two damage models are used for fatigue life prediction, although other damage parameters can easily be adopted. In the first model, the range of maximum principal strain is used as a damage parameter (Eq. (3)), which is reasonable when the principal direction remains fixed. The other parameter is the CXH model (Eq. (4)), which uses normal and shear components of stress and strain on the critical plane and it is suggested as a best parameter by Wang *et al.*[2] Even if these two models use the same symbols of model constants $K$ and $d$, because the damage parameters (the left-hand side) are different, model constants may have different values under the same loading conditions, such as uniaxial loading.

$$\textit{Damage parameter} = K\left(2N_f\right)^d \tag{2}$$

$$\Delta\varepsilon^{\max} = K\left(2N_f\right)^d \tag{3}$$

$$\Delta\sigma_1\Delta\varepsilon_1^{\max} + \Delta\gamma_1\Delta\tau_1 = K\left(2N_f\right)^d \tag{4}$$

In Eq. (2), $K$ and $d$ are the fatigue life prediction coefficients and $N_f$ is the number of cycles to fatigue failure. In Eqs (3) and (4), $\Delta\varepsilon^{\max}$ is the range of maximum principal strain, and $\Delta\varepsilon_1^{\max}$, $\Delta\sigma_1$, $\Delta\gamma_1$ and $\Delta\tau_1$ are the ranges of normal strain, normal stress, shear strain, and shear stress on a critical plane, respectively. Note that the parameters, $K$ and $d$, in Eq. (3) are different from those in Eq. (4). For example, the damage parameter in Eq. (3) is in the unit of strain, while the damage parameter in Eq. (4) is in the unit of strain energy density.

Applying the damage parameter to the history of stress and strain requires converting the history to a sum of unit cycles. Typically, the rainflow counting method is used for this purpose. The standard rainflow counting method is enough for the damage parameter with one component, such as the peak maximum principal strain in Eq. (3), but a special counting method is necessary for the damage parameter of multicomponents, such as the CXH model in Eq. (4). In this paper, the multicomponents rainflow counting method is developed for the CXH damage parameter, which not only keeps the standard procedure of the rainflow counting method using the history of one component but also includes the effect of the history of other components, which is conceptually explained in Fig. 3.

In the case of CXH model, the four components, two stresses and two strains in Eq. (4), need to be considered in rainflow counting. The idea is simple in a sense that the rainflow counting with multicomponents still has a main component and several sub-components. This is based on experimental observation in Wang *et al.*[2], where the cycle is counted based on the main component (in this case, maximum principal strain). For a given cycle of the main component, the model requires the range of sub-components. Therefore, standard rainflow counting is applied to the main component, $\Delta\varepsilon_1^{\max}$, and it is assumed that the start/end points of sub-components of each cycle are identical to those of the main component.

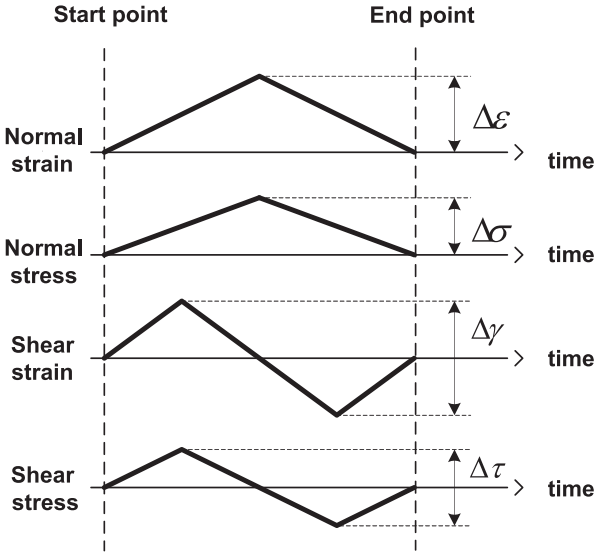


**Fig. 3** Multicomponent rainflow counting for stress and strain range of unit cycle.

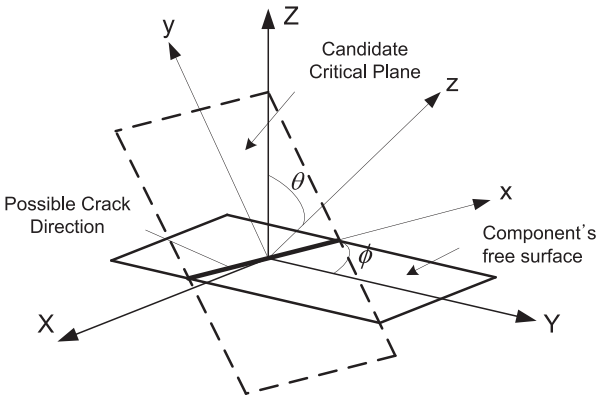


**Fig. 4** Definition of a critical plane for a fatigue failure.

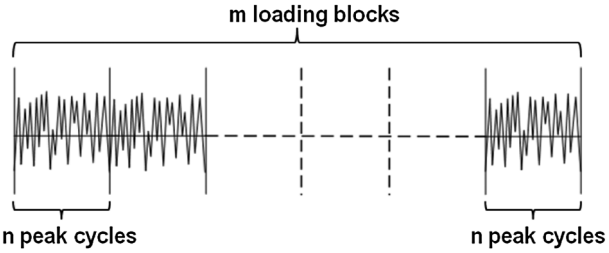


**Fig. 5** Loading blocks of transient loads.

Sub-components' maximum and minimum values are estimated between the start and end points. In Fig. 3, normal strain is the main component, and other components are sub-components.

In the CXH model, the amplitude of the damage parameter depends on the combination of multicomponents. Even if a uniaxial load is applied, the state of stress can be complicated, and the principal direction can be changed along the load path. Therefore, the critical plane method is applied to find the plane that maximizes the damage parameter in Eq. (4). A critical plane is defined by the rotation angles on a free surface, and it is conceptually illustrated in Fig. 4. Generally, the crack is generated on the free surface of a body and the direction of a crack candidate plane can be estimated using two angles, $\theta$ and $\phi$, which define the rotated axes $x$–$y$–$z$ in Fig. 4. The angle $\phi$ has a range from 0° to 180°, and the angle $\theta$ has a range from 0° to 90°. The transformation of stresses and strain from a free surface to a candidate critical plane is expressed in Eq. (5).

$$\boldsymbol{\sigma}_L = \mathbf{T}^T \boldsymbol{\sigma}_G \mathbf{T},\ \boldsymbol{\varepsilon}_L = \mathbf{T}^T \boldsymbol{\varepsilon}_G \mathbf{T} \tag{5}$$

$$\mathbf{T} = \begin{bmatrix} -\sin\theta & -\cos\theta\cos\varphi & \sin\theta\cos\varphi \\ \cos\theta & -\cos\theta\sin\varphi & \sin\theta\sin\varphi \\ 0 & \sin\theta & \cos\theta \end{bmatrix}$$

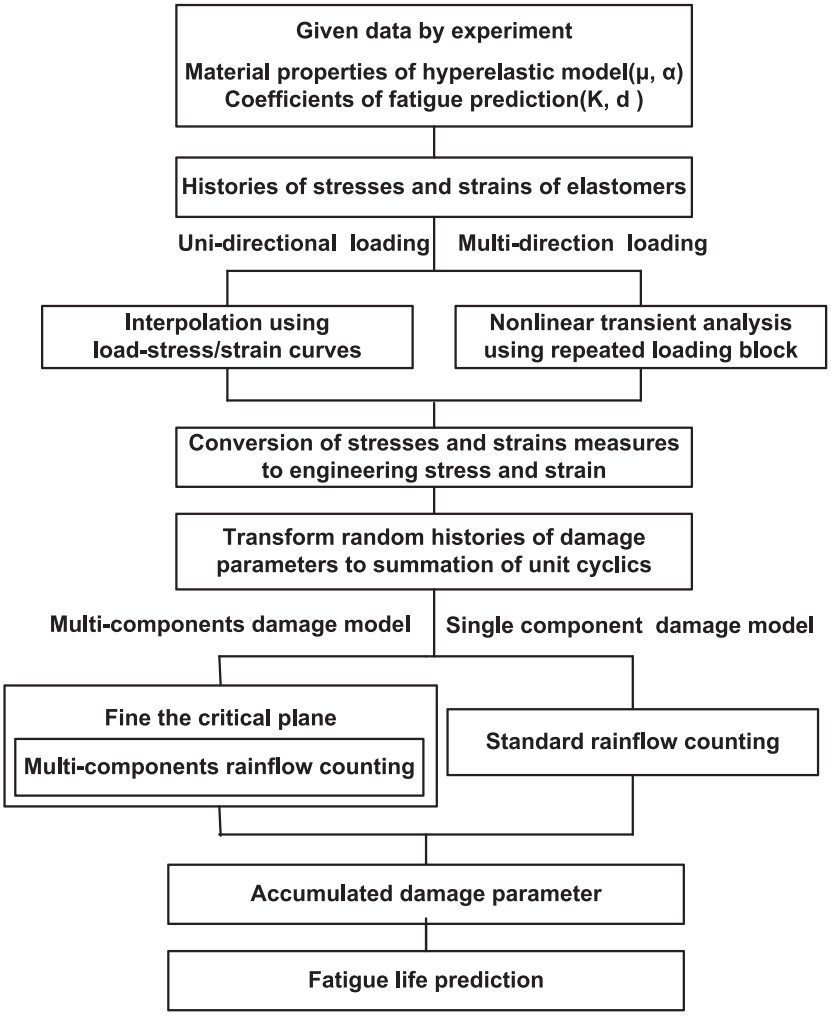


**Fig. 6** Flowchart for fatigue life prediction of elastomers.

$\boldsymbol{\sigma}_G$, $\boldsymbol{\varepsilon}_G$: Stresses and strains of a free surface plane
$\boldsymbol{\sigma}_L$, $\boldsymbol{\varepsilon}_L$: Stresses and strains of a candidate critical plane

The Miner's rule is used to estimate total damage from the sum of all cycles. For the multicomponents damage parameter, the Miner's rule in Eq. (6) is applied for each cycle, and elastomers are assumed to fail when the accumulated damage becomes 1.0. In Eq. (6), $m$ is the number of repeated loading blocks as shown in Fig. 5, $N_i$ is the number of life cycles until failure for $i$-th peak loading, and n is the number of peaks in a loading block. When a loading block is repeated, the histories of stress and strain need to be calculated only within a block because these histories are also repeated in other blocks.

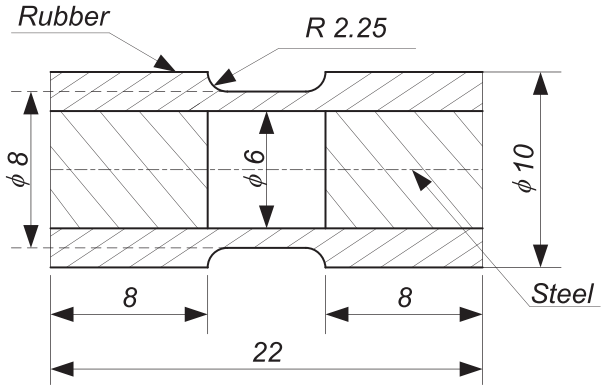


**Fig. 7** Dimension of the specimen (unit: mm).

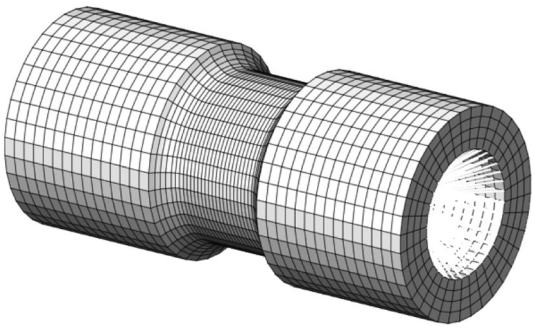

**Fig. 8** FEA model of the specimen.

$$\text{Total Damage} = \text{m}\times\left\{\sum_{i=1}^{2n}\frac{1}{2N_i}\right\} \tag{6}$$

## NUMERICAL FATIGUE PREDICTION OF ELASTOMERS

Figure 6 shows a flowchart of numerical procedure for predicting the fatigue life of elastomers. It has all of the processes that are necessary for fatigue prediction, except for determination of material parameters. The numerical simulations follow the flowchart in Fig. 6.

### Numerical simulation for fatigue life prediction of elastomers

The numerical simulations in this paper are based on the experiments performed by Wang *et al.*[2] Therefore, the properties of the elastomers and the experimental results cited from the paper are used. The dimensions of the elastomer specimen and the numerical model are shown in Figs 7 and 8. The steel connected with the elastomers are modelled by rigid link boundary conditions, and displacement loads are applied at the centres of rigid link groups.

For the hyperelastic behaviour of the elastomer, the Ogden constitutive model is used, whose basic equations are given in Appendix. The material constants of the Ogden model obtained from experiments are shown in Table 1 when $N = 3$. The material constants are modified to include the Mullins effect. The fatigue model coefficients, $K$ and $d$, are determined from unidirectional and multidirectional loadings (Table 2), which depend on the fatigue damage parameters. Experimental data from paths 1 and 2 are used to calculate fatigue model coefficients, while the data from path 3 are used for validation. The material constants and the fatigue model coefficients obtained from experimentation are used in the fatigue life prediction using numerical methods. The numerical methods are performed by the displacement–control method as with the experiments in Wang *et al.*[2] The comparisons between experiments and numerical methods of fatigue life predictions by the maximum principal strain model and the CXH model are shown in Figs 9 and 10, respectively. The results of unidirectional loadings are shown in Fig. 9(a) and Fig. 10(a), and the

**Table 2** Fatigue model coefficients, $K$ and $d$, for different loadings and damage models

| | Unidirectional tests | | Multidirectional tests | |
|---|---|---|---|---|
| Damage criteria | $K$ | $d$ | $K$ | $d$ |
| Peak max. principal strain | 16.12 | −0.218 | 12.87 | −0.201 |
| CXH model | 177.13 (MPa) | −0.357 | 134.73 (MPa) | −0.339 |

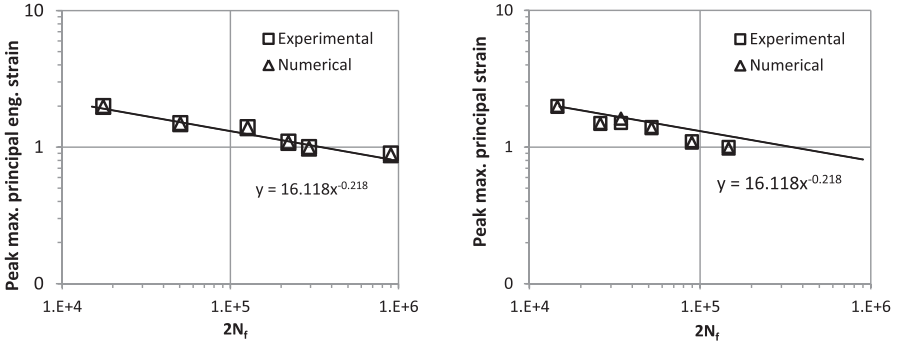


(a) Uni-directional loading test (Path 1) (b) Multi-directional loading test (Path 2 & Path3)

**Fig. 9** Correlation by the peak maximum principal engineering strain model (experimental data from Wang *et al.* [2]).

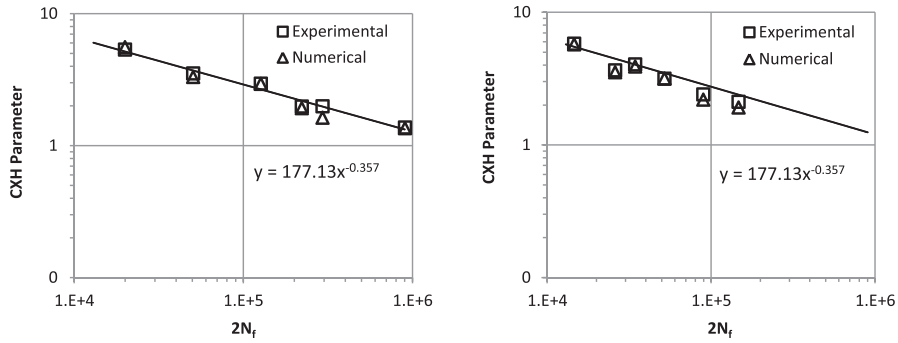


(a) Uni-directional loading (Path 1) (b) Multi-directional loading (Path 2 & Path 3)

**Fig. 10** Correlation by the CXH model (experimental data from Wang *et al.*[2]).

results of multidirectional loadings are shown in Fig. 9(b) and Fig. 10(b). The fatigue model coefficients of two criteria are estimated by a regression curve using involution equation, which were used in the maximum principal engineering strain model and the CHX model. In the case of unidirectional loading test, the correlation coefficient between the maximum principal strain criterion and CXH criterion is 0.92, while the multidirectional loading test, it is 0.95. Therefore, it can be seen that the proposed numerical model can simulate the experimental conditions. Table 3 compares damage parameters from experiments and numerical methods

**Table 3** Fatigue prediction results by experiments and numerical methods (experimental data from Wang *et al.*[2])

| Loading path | $\varepsilon_{min}$ (%) | $\varepsilon_{max}$ (%) | $\gamma_{min}$ (%) | $\gamma_{max}$ (%) | Cycles to failure | Damage parameters | | | |
|---|---|---|---|---|---|---|---|---|---|
| | | | | | | Peak maximum principal engineering strain | | CXH model | |
| | | | | | | Experiment | Numerical | Experiment | Numerical |
| 1 | 0 | 200 | 0 | 0 | 10 000 | 2.00 | 1.97 | 5.33 | 5.55 |
| | 0 | 150 | 0 | 0 | 25 250 | 1.50 | 1.47 | 3.52 | 3.31 |
| | 0 | 140 | 0 | 0 | 63 500 | 1.40 | 1.37 | 2.95 | 2.93 |
| | 0 | 110 | 0 | 0 | 110 000 | 1.10 | 1.07 | 1.98 | 1.92 |
| | 0 | 100 | 0 | 0 | 147 050 | 1.00 | 0.97 | 1.98 | 1.63 |
| | 0 | 90 | 0 | 0 | 450 800 | 0.90 | 0.87 | 1.37 | 1.35 |
| 2 | 0 | 200 | −35 | 35 | 7300 | 2.00 | 1.97 | 5.80 | 5.73 |
| | 0 | 150 | −35 | 35 | 13 000 | 1.50 | 1.47 | 3.65 | 3.53 |
| | 0 | 140 | −35 | 35 | 26 000 | 1.40 | 1.37 | 3.15 | 3.16 |
| | 0 | 110 | −35 | 35 | 44 800 | 1.10 | 1.07 | 2.40 | 2.19 |
| | 0 | 100 | −35 | 35 | 73 499 | 1.00 | 0.97 | 2.11 | 1.91 |
| 3 | 0 | 150 | −35 | 35 | 17 180 | 1.50 | 1.61 | 4.03 | 3.90 |

with a good agreement for all three paths. Damage parameters of the maximum principal strain model in Table 3 are not changed between paths 1 and 2, because the damage parameter only depends on the maximum principal strain. On the other hand, damage parameters of the CXH model include both normal and shear components of stress and strain. Therefore, in multidirectional loadings, the values of damage parameters are higher than those of unidirectional loadings at the same normal deformation.

It is acknowledged that more complicated load paths than those in Fig. 11 can be used to build a robust fatigue model. For more complicated load paths, readers are referred to the reference by Saintier *et al.*[8,9] and Zarrin-Ghalami *et al.* [10,11]. However, complicated load paths can increase the possibility of experimental error as well as cost.

## Fatigue life prediction of an engine mount

As a practical example, the fatigue life of a rubber engine mount is calculated using the proposed method. The same material properties in Table 1 and CXH fatigue coefficients in Table 2 are used for the rubber part. The inner and outer bushings are made of aluminium. The dimensions of the engine mount model are shown in Fig. 12(a). Plane stress condition is assumed with a unit thickness. A block loading with 50 cycles, shown in Fig. 12(b), is repeatedly applied in the x-direction at the centre of the inner bushing, that is, unidirectional loading. A commercial finite element analysis software[15], MIDAS NFX (Gyeonggi-do, Korea), is used to carry out nonlinear analysis. Figure 13 shows the contour plot of the maximum principal true strain at the maximum load magnitude. It is noted that the maximum value occurs (near the 140° region) in the inner bushing (point A in Fig. 13). Because applied loading is unidirectional, the stress and strain histories can be calculated either using interpolation from a single nonlinear analysis or using nonlinear transient analysis with a loading block. Figure 14(a) and (b) shows the time history of

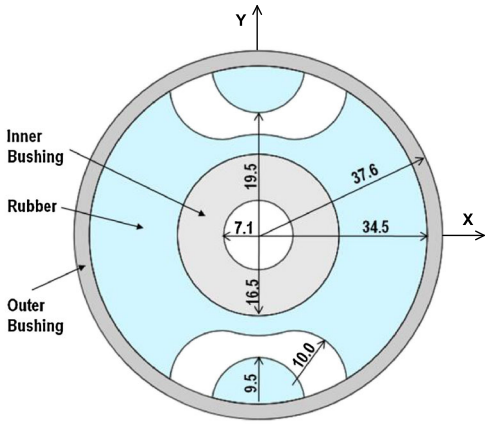


(a) The general shape and dimension of the rubber mount

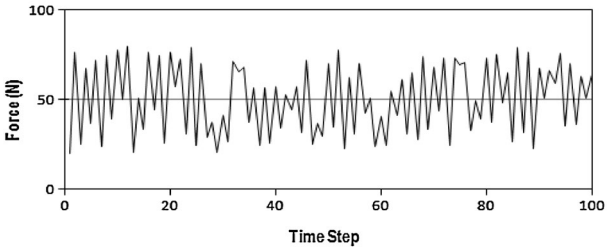


(b) Random loading of 50 cycles

**Fig. 12** Dimension of the rubber mount and an assumed practical loading.

the normal true strain and stress at point A and its critical plane from the two methods. It is noted that both results are very close to each other.

Once the stress and strain histories are available, fatigue life prediction is possible by defining the history of damage parameters. In the critical plane method, the range of angles $\phi$ and $\theta$ are divided by 10° increments, and damage parameters are calculated at each angle. After rainflow counting, the accumulated damage of the loading block is calculated using the Miner's rule in Eq. (6). A damage ratio is defined as an inverse of the number

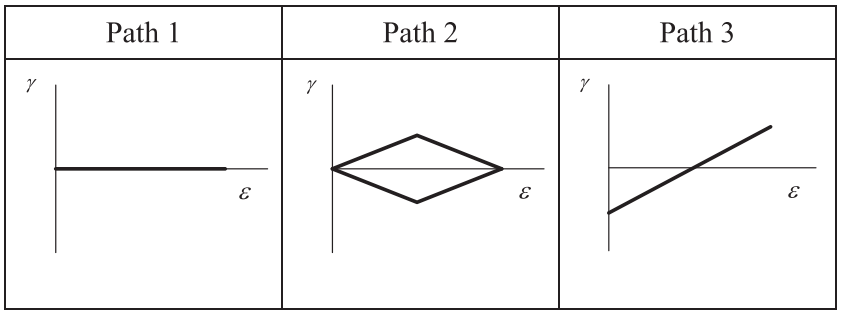


**Fig. 11** Unidirectional and multidirectional loading paths.

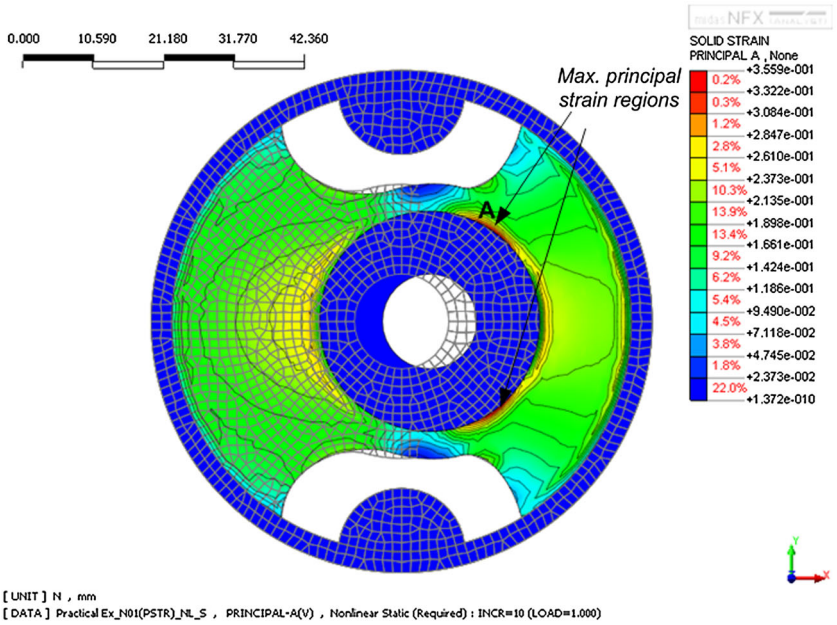


**Fig. 13** Maximum principal true strain distribution at the maximum load.

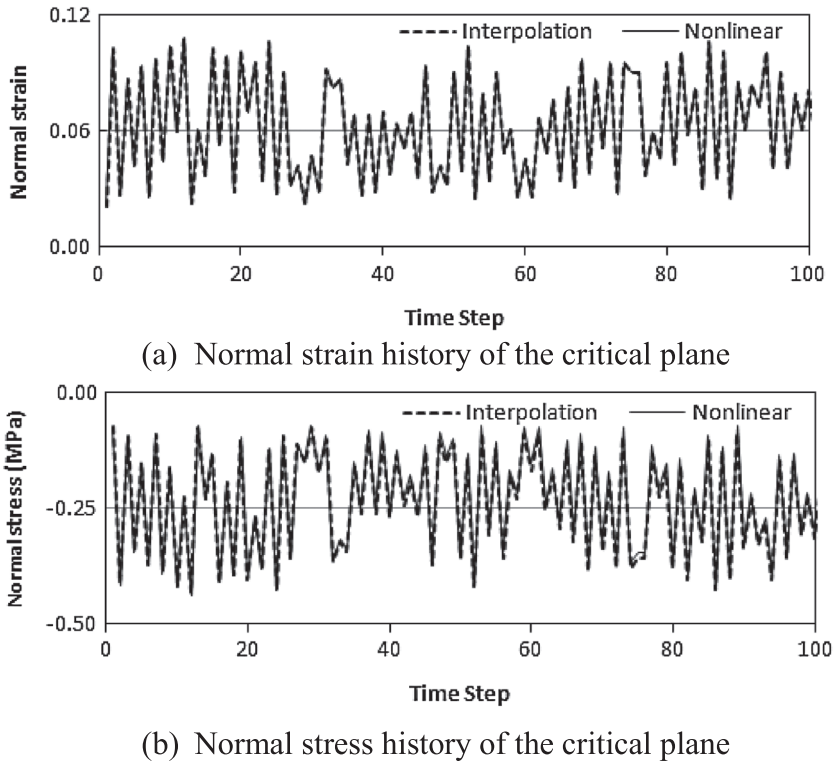


**Fig. 14** Normal strain and stress of the critical plane at point A.

of cyclic loading blocks when the fatigue failure occurs. Figure 15 shows the plot of block damage ratio as a function of angles $\phi$ and $\theta$. In this example, the critical plane is determined by the rotation of 140° along the z-direction and the rotation of 0° along the y-direction. The damage ratios by the CXH model for fatigue prediction criteria are listed in Table 4. The damage ratio is defined as an inverse of the number of cyclic loading blocks when

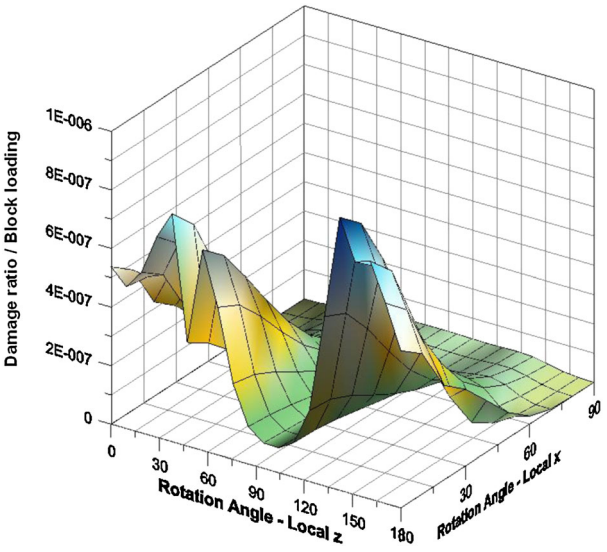


**Fig. 15** Damage ratios of a given block loading for each critical plane.

**Table 4** Damage ratios for a given block cyclic loading for the CXH criteria

| Methods | Unidirectional loading test ($K$, $d$) | Multidirectional loading test ($K$, $d$) |
|---|---|---|
| Linear interpolation | $8.764 \times 10^{-7}$ | $7.168 \times 10^{-7}$ |
| Nonlinear transient | $8.922 \times 10^{-7}$ | $7.329 \times 10^{-7}$ |

the fatigue failure occurs, that is, the fatigue life is (1/damage ratios) blocks. This definition is consistent with Miner's damage accumulation rule. There is around a 2% difference of damage ratios between linear interpolation scheme and the nonlinear transient method. However, the cost of solution is not comparable because the linear interpolation scheme using the relationship between stresses and strain versus loadings needs only around 10 steps from minimum to maximum loadings, while the nonlinear transient analysis over full time loadings is necessary for the nonlinear transient procedure.

## CONCLUSIONS

The numerical methods for fatigue life prediction of elastomers under variable amplitude loadings are presented. The suggested numerical methods can be applicable for elastomers of any complicated structure using the material properties of hyperelastic behaviour and fatigue life prediction coefficients given by experiments. The characteristic properties of elastomers, such as hyperelastic behaviour and Mullins effect, are summarized. Considering nonlinear behaviour of elastomers, an efficient interpolation scheme using load stress/strain curves is investigated in unidirectional loadings, and it can greatly reduce the cost of solution of histories of stresses and strains under time-varying loadings. For multidirectional loading, using a repeated loading block with nonlinear transient analysis is suggested. The difference of measure of stresses and strains between experiments and numerical methods is explained, and the conversion methods between measures are summarized. The multicomponents rainflow counting for a damage parameter having multicomponents of stresses and strains is developed, and the method is applied with the critical plane method for the CXH damage parameter. In the comparison between experiments and numerical methods, the fatigue life predictions of numerical methods show good agreement with those of experiments under unidirectional and multidirectional loadings. In addition, the procedure of the suggested numerical methods is applied for a practical example, an engine rubber mount. It is shown that the numerical results matched with experimental data with uniaxial and multiaxial loadings, which mean that the suggested numerical method can simulate the experimental results well. In addition, because the damage parameters of the CXH model include both normal and shear components of stress and strain, in multidirectional loadings, the values of damage parameters are higher than that of unidirectional loadings at the same normal deformation. In practical application, it is shown that the proportional loading can save significant amount of computational time compare with nonlinear transient case.

## Acknowledgements

The proposed research has partly been supported by MIDAS IT. This support is greatly appreciated by the authors.

## REFERENCES

1 Collins, J. (1993) Failure of Materials in Mechanical Design: Analysis, Prediction Prevention, 2nd ed, The Ohio State University: Columbus, OH.
2 Wang, Y., Yu, W., Chen, X. and Yan, L. (2008) Fatigue life prediction of vulcanized natural rubber under proportional and non-proportional loading. *Fatigue Fract. Eng. Mater. Struct.*, **31**, 38–48.
3 Li, Q., Zhao, J. and Zhao, B. (2009) Fatigue life prediction of a rubber mount based on test of material properties and finite element analysis. *Engng, Failure Anal*, **16**, 2304–2310.
4 Kim, W., Lee, H., Kim, J. and Koh, S. (2004) Fatigue life estimation of an engine rubber mount. *Int. J. Fatigue*, **26**, 553–560.
5 Mars, W. and Fatemi, A. (2005) Multiaxial fatigue of rubber: part I: equivalence criteria and theoretical aspects. *Fatigue Fract. Eng. Mater. Struct.*, **28**, 515–522.
6 Mars, W. and Fatemi, A. (2005) Multiaxial fatigue of rubber: part II: experimental observations and life predictions. *Fatigue Fract. Eng. Mater. Struct.*, **28**, 523–538.

7 Mars, W. and Fatemi, A. (2006) Multiaxial stress effects on fatigue behavior of filled natural rubber. *Int. J. Fatigue*, **28**, 521–529.
8 Saintier, N., Cailletaud, G. and Piques, R. (2006) Crack initiation and propagation under multiaxial fatigue in a natural rubber. *Int. J. Fatigue*, **28**, 61–72.
9 Saintier, N., Cailletaud, G. and Piques, R. (2006) Multiaxial fatigue life prediction for a natural rubber. *Int. J. Fatigue*, **28**, 530–539.
10 Zarrin-Ghalami, T. and Fatami, A. (2013) Multiaxial fatigue and life prediction of elastomeric components. *Int. J. Fatigue*, **55**, 92–101.
11 Zarrin-Ghalami, T. and Fatami, A. (2013) Cumulative fatigue damage and life prediction of elastomeric components. *Fatigue Fract. Eng. Mater. Struct.*, **36**, 270–279.
12 Smith, R., Waston, P. and Topper, T. (1970) A stress–strain parameter for fatigue of metals. *J. Mater.*, **5**, 767–778.
13 Chen, X., Xu, S. and Huang, D. (1999) Critical plane-strain energy density criterion of multiaxial low-cycle fatigue life. *Fatigue Fract. Eng. Mater. Struct.*, **22**, 679–686.
14 Fatemi, A. and Socie, D. (1988) A critical plane approach to multiaxial fatigue damage including out-of-plane loading. *Fatigue Fract. Eng. Mater. Struct.*, **14**, 149–165.
15 Park, S. and Chung, J. (2011) MIDAS NFX Manual. MIDAS Information and Technology ltd, Seoul, Korea.

## APPENDIX

The basic equations of the Ogden model for hyperelastic behaviour of elastomers and several relations between experimental results measures and numerical methods measures are listed in this Appendix.

Ogden Model for Hyperelastic behaviour

$$W = \sum_{i=1}^{N} \frac{\mu_i}{\alpha_i}\left(\lambda_1^{\alpha_i} + \lambda_2^{\alpha_i} + \lambda_3^{\alpha_i} - 3\right)$$

$$\mathbf{S} = \frac{\partial W}{\partial \mathbf{E}}$$

$$\mathbf{E} = \frac{1}{2}\left(\mathbf{F}^T\mathbf{F} - 1\right)$$

Second Piola–Kirchhoff stress

$$\mathbf{P} = \mathbf{S}\mathbf{F}^T$$

Cauchy stress

$$\mathbf{P} = \mathcal{J}\mathbf{F}^{-1}\boldsymbol{\sigma}$$

Green–Lagrange strain

$$\mathbf{E} = \frac{1}{2}\left(\mathbf{F}^T\mathbf{F} - 1\right)$$

$$2\mathbf{E} + 1 = \mathbf{F}^T\mathbf{F} = \mathbf{C} = \mathbf{U}^T\mathbf{R}^T\mathbf{R}\mathbf{U} = \mathbf{U}^T\mathbf{U}$$

$$= \boldsymbol{\Phi}\Lambda\boldsymbol{\Phi}^T \quad (\mathbf{F} = \mathbf{R}\mathbf{U})$$

$$\boldsymbol{\Phi} = [\,\mathbf{n}_1 \quad \mathbf{n}_2 \quad \mathbf{n}_3\,],\ \Lambda = \begin{bmatrix} \lambda_1 & 0 & 0 \\ 0 & \lambda_2 & 0 \\ 0 & 0 & \lambda_3 \end{bmatrix}$$

$$\boldsymbol{\varepsilon}_{Eng} = \left(\sqrt{\lambda_1} - 1\right)\mathbf{n}_1\mathbf{n}_1^T + \left(\sqrt{\lambda_2} - 1\right)\mathbf{n}_2\mathbf{n}_2^T + \left(\sqrt{\lambda_3} - 1\right)\mathbf{n}_3\mathbf{n}_3^T$$

Logarithmic strain

$$\boldsymbol{\varepsilon}_{Log} = \ln(\lambda_1)\mathbf{n}_1\mathbf{n}_1^T + \ln(\lambda_2)\mathbf{n}_2\mathbf{n}_2^T + \ln(\lambda_3)\mathbf{n}_3\mathbf{n}_3^T$$

$$= \boldsymbol{\Phi}_L\Lambda_L\boldsymbol{\Phi}_L^T\boldsymbol{\Phi}_L = [\,\mathbf{n}_{L,1} \quad \mathbf{n}_{L,2} \quad \mathbf{n}_{L,3}\,],\ \Lambda_{Log}$$

$$= \begin{bmatrix} \lambda_{L,1} & 0 & 0 \\ 0 & \lambda_{L,2} & 0 \\ 0 & 0 & \lambda_{L,3} \end{bmatrix} \boldsymbol{\varepsilon}_{Eng} = \left(e^{\lambda_{L,1}} - 1\right)\mathbf{n}_{L,1}\mathbf{n}_{L,1}^T + \left(e^{\lambda_{L,2}} - 1\right)\mathbf{n}_{L,2}\mathbf{n}_{L,2}^T + \left(e^{\lambda_{L,3}} - 1\right)\mathbf{n}_{L,3}\mathbf{n}_{L,3}^T$$